



Contents lists available at ScienceDirect

# Spectrochimica Acta Part A: Molecular and Biomolecular Spectroscopy

journal homepage: [www.elsevier.com/locate/saa](http://www.elsevier.com/locate/saa)

## A water-soluble molecular probe with aggregation-induced emission for discriminative detection of Al<sup>3+</sup> and Pb<sup>2+</sup> and imaging in seedling root of *Arabidopsis*

Pengfei Xu<sup>1</sup>, Zhiyi Bao<sup>1</sup>, Chenyi Yu, Qianqian Qiu, Mengru Wei, Wenbin Xi, Zhaosheng Qian, Hui Feng\*

Key Laboratory of the Ministry of Education for Advanced Catalysis Materials, College of Chemistry and Life Sciences, Zhejiang Normal University, Jinhua 321004, People's Republic of China

### ARTICLE INFO

#### Article history:

Received 15 May 2019

Received in revised form 18 June 2019

Accepted 30 June 2019

Available online 02 July 2019

#### Keywords:

Aggregation-induced emission (AIE)

Molecular probe

Aluminum ion

Lead ion

Imaging

### ABSTRACT

Luminogens with aggregation-induced emission (AIE) have been used to develop a new type of molecular probes based on analyte-triggered aggregation, but it still remains a challenge to design water-soluble AIE-active probe for specific detection of metal ions. Herein, we designed and synthesized a water-soluble molecular probe with AIE property for discriminative detection of aluminum ion and lead ion. Four carboxylic acid groups were incorporated into a tetraphenylethylene unit to enhance the coordination affinity and increase water-solubility in aqueous solution. The designed probe can be selectively lighted up by aluminum ion and lead ion via coordination-triggered AIE process. Discrimination of aluminum ion and lead ions based on the probe can be achieved in quantitative manner with the assistance of suitable masking reagents. This probe was further used to image aluminum ions in living cells of seedling roots of *Arabidopsis*, and the results showed that this probe is capable of imaging aluminum ions in living cells avoiding the interference of lead ions, and is suited for long-term imaging due to its excellent photostability. This work expands the application scope of AIE-active probes in discriminative detection of metal ions, and provides a design direction for water-soluble AIE probes to avoid the false signals from self-precipitation under physiological conditions.

© 2019 Elsevier B.V. All rights reserved.

### 1. Introduction

The accurate measurement of metal ions is a persistent challenge for chemists because some lighter metal ions play indispensable roles in diverse biological processes while exposure to heavier and toxic metal ions has increased with industrialization. Aluminum as the third most abundant element in the earth crust, has continuously entered ecosystem and biosphere due to the increase of acid rains [1]. Present evidence has indicated that the intake of aluminum ion causes a significant toxicity to organisms including plants and human [2,3]. Moreover, lead ion is another significant pollutant occurred widely in environments because of its highly toxic feature to organisms [4,5]. The quantification and imaging of these toxic metal ions generally require accurate and specific optical methods relying on fluorogenic indicators [6,7]. Despite diverse fluorescent probes have been developed for Al<sup>3+</sup> and Pb<sup>2+</sup>, most of them were based on conventional dyes with aggregation-induced quenching (ACQ) feature. These ACQ fluorophores frequently suffer from an appreciable decline in brightness

caused by aggregation and significant photobleaching under the long-term irradiation of excitation light.

Aggregation-induced emission luminogens (AIEgens) have shown great power and promising prospect in sensing and imaging since its discovery by Tang group [8,9]. In contrast with ACQ fluorogens, AIEgens have weak emission in dissolved state, but emit intense fluorescence in aggregated or solid state [10]. This unique property of AIEgens allows to establish a novel type of detection strategy based on aggregation-induced emission [11,12], and these AIE-active probes exhibit better photostability in long-term imaging than existing ACQ probes [13]. As a result, a variety of AIE-active probes for detecting metal ions including Ag<sup>+</sup> [14,15], Hg<sup>2+</sup> [16,17], Zn<sup>2+</sup> [18–21], and Ca<sup>2+</sup> [22,23] based on coordination-triggered aggregation processes have been developed, and a number of fluorometric methods for Al<sup>3+</sup> based on diverse AIEgens have also reported [24–31]. However, most of these reported AIE-active molecular probes have poor water-solubilities, and thus specific organic solvents such as DMSO and THF are required for them to quantify and image Al<sup>3+</sup> because of their poor solubility in water. The low solubility of AIE probes in aqueous solution probably causes false signals from their self-precipitation inside live cells during the imaging process, which will greatly impact the sensitivity and accuracy of tracking Al<sup>3+</sup> in biosystems. In addition, AIE-active probes for Pb<sup>2+</sup> are very

\* Corresponding author.

E-mail address: [fenghui@zjnu.cn](mailto:fenghui@zjnu.cn) (H. Feng).<sup>1</sup> These authors contributed to this work equally.

rare currently [32–34], and dual-functional indicators for discriminative quantitation of  $\text{Al}^{3+}$  and  $\text{Pb}^{2+}$  in a facile way have not reported till now.

In this contribution, we designed and synthesized a water-soluble molecular probe for quantification of  $\text{Al}^{3+}$  and  $\text{Pb}^{2+}$  based on ion-triggered aggregation-induced emission. Four carboxylic acid groups were incorporated into a tetraphenylethylene unit in the probe. The introduction of these carboxylic acid groups not only endows excellent solubility of the probe in water but also provides the recognition units for target metal ions. As shown in Scheme 1, the probe TPE-4CO<sub>2</sub>Na can be effectively assembled by  $\text{Al}^{3+}$  and  $\text{Pb}^{2+}$  via their coordination reactions between metal ions and carboxylic acid groups. With the assistance of masking agents, the probe TPE-4CO<sub>2</sub>Na was used for discriminative detection of  $\text{Al}^{3+}$  or  $\text{Pb}^{2+}$  in a fluorescence turn-on manner. The imaging performance of the probe for  $\text{Al}^{3+}$  in live cells was further evaluated in *Arabidopsis thaliana*.

## 2. Experimental

### 2.1. Materials and reagents

Triple-distilled water was utilized throughout the whole experimental process. 4,4-Dimethoxybenzophenone, Zn dust, boron tribromide and ethyl chloroacetate were purchased from Sigma-Aldrich Company (Shanghai, China). HEPES solution (10 mM, pH 7.0) was used as the buffer solution. All reagents were of analytical grade and without any further purification.

### 2.2. Synthesis of 1,1,2,2-tetrakis(4-methoxyphenyl)ethene (Compound 2)

A typical procedure for synthesis of Compound 2 was as follows. Zn dust (1.84 g, 28 mmol) and  $\text{TiCl}_4$  (1.58 mL, 14 mmol) were refluxed for 2 h in 50 mL of dry THF under  $\text{N}_2$  atmosphere. A solution of 4,4-dimethoxybenzophenone (1.50 g, 7.0 mmol) in dry THF (20 mL) was added to the preceding suspension, and then the reaction was refluxed at 80 °C for 12 h. An aqueous solution containing 10%  $\text{K}_2\text{CO}_3$  (50 mL) was added after the reaction mixture was cooled down to room temperature. The resulting product was extracted with ethyl acetate. The solvent was evaporated under vacuum and the crude product was purified by a silica gel column using hexane-ethyl: acetate (1:1, v/v)

as the eluent. Compound 2 was obtained in 70% yield (1.01 g). <sup>1</sup>H NMR (600 MHz,  $\text{CDCl}_3$ )  $\delta$  (ppm) 6.93 (d,  $J$  = 6 Hz, 8H), 6.64 (d,  $J$  = 6 Hz, 8H), 3.77 (s, 12H). <sup>13</sup>C NMR (150 MHz,  $\text{CDCl}_3$ )  $\delta$ (ppm) 158.96, 138.08, 138.07, 133.75, 114.19, 56.28. HRMS (ESI)  $m/z$ : [ $M + \text{K}^+$ ] 491.1633, (calcd. for  $\text{C}_{30}\text{H}_{28}\text{O}_4$ , 452.0653).

### 2.3. Synthesis of 1,1,2,2-tetrakis(4-hydroxyphenyl)ethylene (Compound 3)

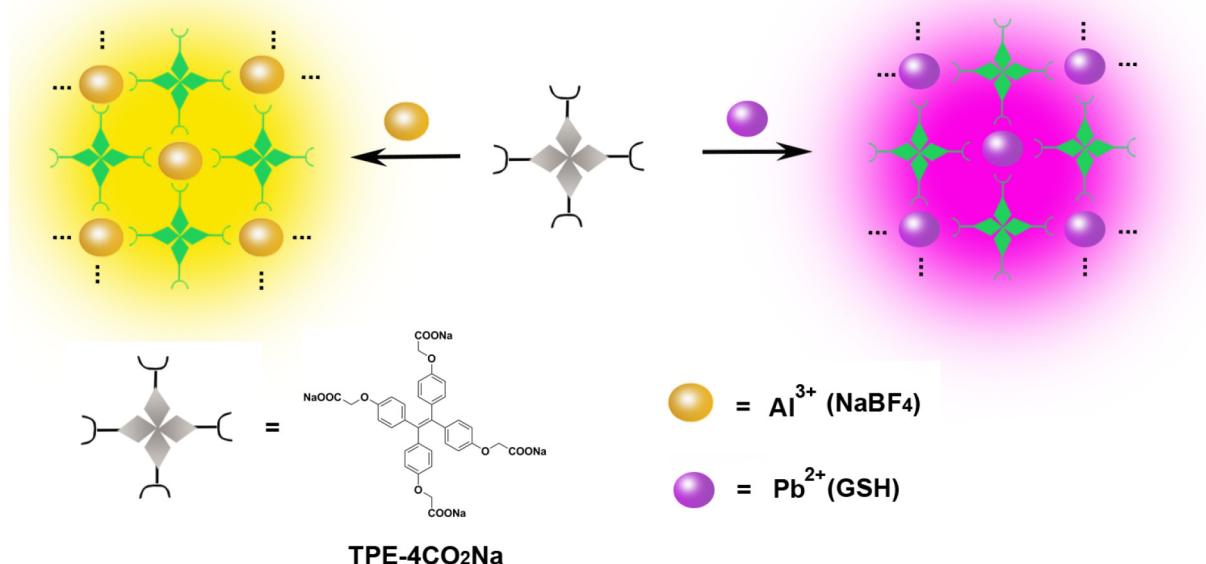
A certain amount of  $\text{BBr}_3$  (4 mL, 44.2 mmol) was first added in 50 mL of dry DCM solution containing Compound 2 (2.00 g, 4.42 mmol) at  $-20$  °C. The mixture was stirred for 40 h at room temperature, and then was concentrated under vacuum. The mixture was poured into 100 mL water and stirred for 5 min after adding 3 ml ethanol, and then massive white precipitates were generated. The final product was obtained in 97% yield (1.7 g) after filtration and drying. <sup>1</sup>H NMR (600 MHz,  $\text{DMSO}-d_6$ )  $\delta$  9.24 (s, 4H), 6.70 (d,  $J$  = 12 Hz, 8H), 6.48 (d,  $J$  = 12 Hz, 8H). <sup>13</sup>C NMR (150 MHz,  $\text{DMSO}-d_6$ )  $\delta$  155.34, 137.67, 135.05, 131.94, 114.47. HRMS (ESI)  $m/z$ : [ $M + \text{Na}^+$ ] 419.1249, (calcd. for  $\text{C}_{26}\text{H}_{28}\text{O}_4$ , 396.1349).

### 2.4. Synthesis of tetraethyl 2,2',2'',2'''-((ethane-1,1,2,2-tetrakis(benzene-4,1-diyl))tetrakis-(oxy)tetraacetate (Compound 4)

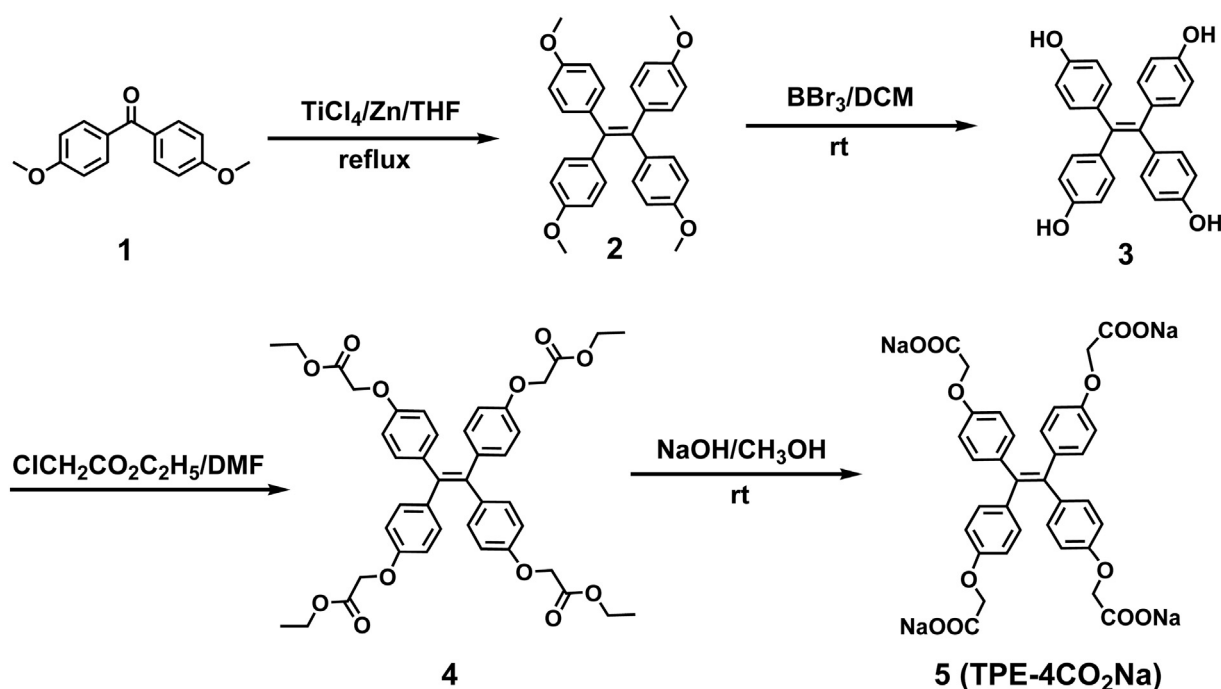
Compound 3 (1.5 g, 3.78 mmol),  $\text{Cs}_2\text{CO}_3$  (8.631 g, 26.49 mmol) and ethyl chloroacetate (3.142 mL, 26.49 mmol) was added in 80 mL DMF, and then the mixture was stirred for 48 h at 80 °C. White precipitates were generated after the mixture was poured into water. The final product was obtained in 90% yield (2.57 g) after washing and drying. <sup>1</sup>H NMR (600 MHz,  $\text{DMSO}-d_6$ )  $\delta$  6.85 (d,  $J$  = 12 Hz, 8H), 6.69 (d,  $J$  = 12 Hz, 8H), 4.68 (s, 8H), 4.15 (q,  $J$  = 18 Hz, 8H), 1.18 (t,  $J$  = 12 Hz, 12H). <sup>13</sup>C NMR (150 MHz,  $\text{DMSO}-d_6$ )  $\delta$  168.68, 155.93, 138.20, 136.77, 131.95, 113.86, 64.60, 60.64, 14.02. HRMS (ESI)  $m/z$ : [ $M + \text{Na}^+$ ] 763.2723, (calcd. for  $\text{C}_{42}\text{H}_{44}\text{O}_{12}$ , 740.2823).

### 2.5. Synthesis of sodium 2,2',2'',2'''-((ethane-1,1,2,2-tetrakis(benzene-4,1-diyl))tetrakis-(oxy)tetraacetate (Compound 5, TPE-4CO<sub>2</sub>Na)

Compound 5 was synthesized by the reaction between Compound 4 (1.3 g, 1.75 mmol) and NaOH (0.28 g, 7 mmol) in 40 ml methanol. The



**Scheme 1.** Schematic Illustration of Discriminative Detection of  $\text{Al}^{3+}$  and  $\text{Pb}^{2+}$  Based on Aggregation-Induced Emission of the Probe TPE-4CO<sub>2</sub>Na with Assistance of Masking Agents.

Scheme 2. Synthetic Route of the Probe TPE-4CO<sub>2</sub>Na.

white precipitates were collected after filtration and drying (95% yield). <sup>1</sup>H NMR (600 MHz, D<sub>2</sub>O) δ 7.03 (d, *J* = 12 Hz, 8H), 6.72 (d, *J* = 6 Hz, 8H), 4.40 (s, 8H). <sup>13</sup>C NMR (150 MHz, D<sub>2</sub>O) δ 176.72, 156.12, 138.81, 137.29, 132.45, 113.74, 66.65. HRMS (ESI) *m/z*: [M-H<sup>+</sup>] 627.1477, (calcd. for C<sub>34</sub>H<sub>28</sub>O<sub>4</sub>, 628.1557).

## 2.6. Discriminative detection of aluminum ion and lead ion based on TPE-4CO<sub>2</sub>Na

For quantitative detection of Al<sup>3+</sup>, a TPE-4CO<sub>2</sub>Na solution with a fixed concentration (20.0 μM) in HEPES buffer (pH 7.0) was first prepared, and then different amounts of Al<sup>3+</sup> in the range of 0.0–650.0 μM were separately added into the preceding TPE-4CO<sub>2</sub>Na solution. The PL spectra of the resulting mixtures were recorded at the excitation of 355 nm using a xenon arc lamp. The quantitative detection of Pb<sup>2+</sup> was performed in a similar procedure using Pb<sup>2+</sup> instead of Al<sup>3+</sup>, and the used amount of Pb<sup>2+</sup> was in the range of 0.0–500.0 μM. Selectivity test of the assay to Al<sup>3+</sup> and Pb<sup>2+</sup> was conducted as follows. A certain amount of each chosen metal cation (100.0 μM) including K<sup>+</sup>, Mg<sup>2+</sup>, Ca<sup>2+</sup>, Ba<sup>2+</sup>, Al<sup>3+</sup>, Pb<sup>2+</sup>, Cd<sup>2+</sup>, Co<sup>2+</sup>, Fe<sup>2+</sup>, Ag<sup>+</sup>, Zn<sup>2+</sup>, Hg<sup>2+</sup>, Cu<sup>2+</sup>, Mn<sup>2+</sup>, Cr<sup>3+</sup> and Fe<sup>3+</sup> was separately added into a TPE-4CO<sub>2</sub>Na solution (20.0 μM) in HEPES buffer, and then the resulting solutions were monitored using fluorescence spectrometer at 480 nm emission. For the discriminative detection of aluminum ion and lead ion, the protocol is same to the normal detection except for the addition of masking reagents. Glutathione and NaBF<sub>4</sub> were separately used to mask the effect of lead ion and aluminum ion, and their concentrations were 100.0 μM. All the detections were repeated at least three times.

## 2.7. Live-cell imaging of aluminum ions in root cells of *Arabidopsis thaliana*

The wild-type (Col-0) seeds of *Arabidopsis thaliana* were surface sterilized and imbibed for 3 days at 4 °C in dark and then sown onto 0.5 × Murashige & Skoog (MS) 1.5% (w/v) agar plates. Seedlings were vertically grown on plates in a climate-controlled growth room (22/20 °C day/night temperature, 16/8-h photoperiod, and 80 μE s<sup>-1</sup> m<sup>-2</sup> light intensity). Five-day-old seedlings with healthy roots were used in this study unless otherwise specified. Fluorescence imaging

experiment was performed on a Leica TCS SP5 model confocal laser scanning microscope (Germany) with an excitation at 355 nm and a variable bandpass emission filter (475–530 nm). Five-day-old seedlings with healthy roots were divided into three groups. The first group was used as mock control. The second group was first treated with 0.5 mM TPE-4CO<sub>2</sub>Na solution for 10 min, and then incubated in an aluminum ion solution (0.5 mM) for 10 min after these seedlings were washed with triple-distilled water. The third groups were treated with 0.5 mM TPE-4CO<sub>2</sub>H in DMSO/water mixed solution for 30 s, and then incubated in an aluminum ion (or lead ion) solution (0.5 mM) for 10 min after washing. All groups were imaged using the confocal laser scanning microscope at the emission range of 475–530 nm. All the photostability experiments were carried out under the radiation of 355 nm and the irradiation time of 1, 3 and 5 min, respectively.

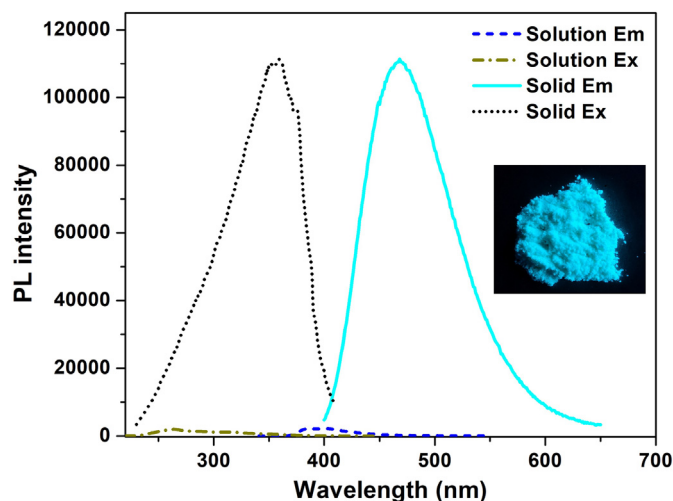


Fig. 1. PL spectra of an aqueous solution and powder of TPE-4CO<sub>2</sub>Na. Inset: A photoimage of TPE-4CO<sub>2</sub>Na powder under UV light.

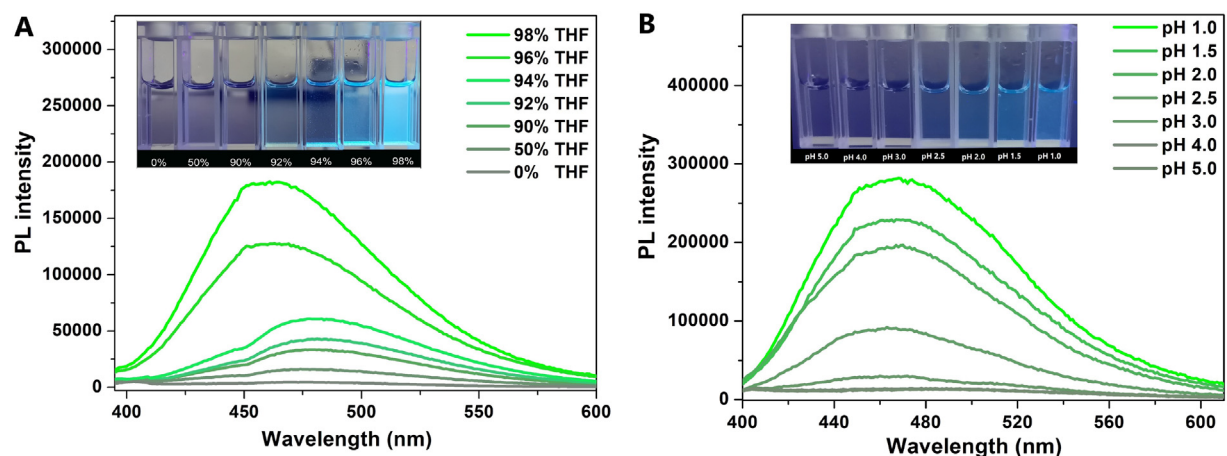


Fig. 2. (A) PL spectra of an aqueous solution of TPE-4CO<sub>2</sub>Na in the presence of different amounts of THF. Inset: Corresponding fluorescence images. (B) PL spectra of an aqueous solution of TPE-4CO<sub>2</sub>Na at different pHs from 1.0 to 5.0. Inset: Corresponding fluorescence images.

### 3. Results and discussion

#### 3.1. Synthesis and characterization of the probe TPE-4CO<sub>2</sub>Na

Tetraphenylethylene as a typical AIE fluorophore was adopted as the signaling unit, and carboxylic acid groups acted as the recognition unit in the probe. Four carboxylic acid groups were introduced to the probe to increase the solubility of the designed probe in water. Scheme 2 shows the synthetic route of the probe TPE-4CO<sub>2</sub>Na. 4,4'-

Dimethoxybenzophenone (1) was used as the starting material to synthesize 1,1,2,2-tetrakis(4-methoxyphenyl)ethylene (2) via a McMurry coupling reaction. 1,1,2,2-Tetrakis(4-hydroxyphenyl)ethylene (3) was generated by the following conversion of hydroxyl groups from methoxy groups through the treatment of BBr<sub>3</sub>. Four carboxylic esters were further introduced via the nucleophilic substitution between (3) and ethyl chloroacetate to produce (4). The probe TPE-4CO<sub>2</sub>Na (5) was finally acquired by the hydrolysis of 4 using NaOH. All the intermediates and the final product were obtained in good yields, and all of

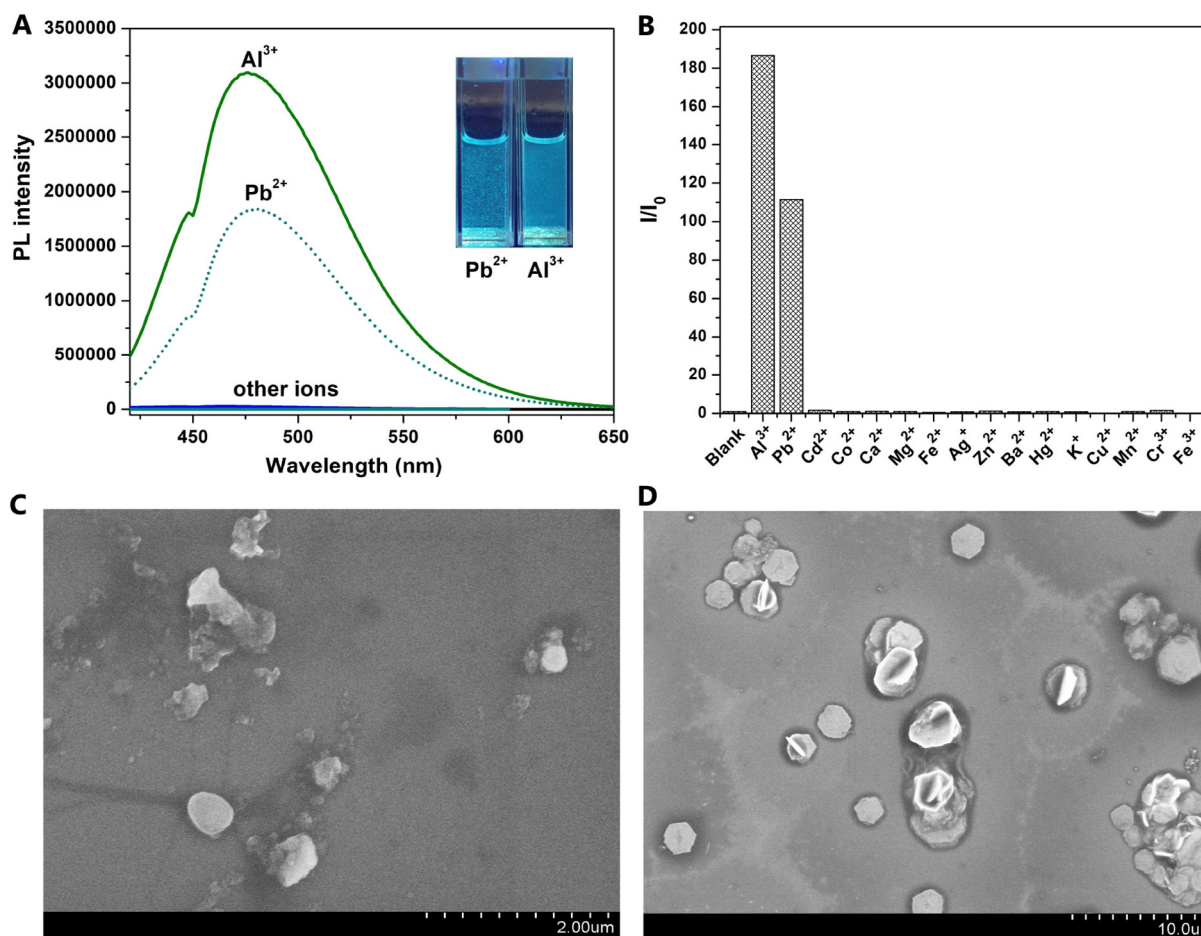


Fig. 3. (A) PL spectra of a HEPES solution of TPE-4CO<sub>2</sub>Na (20.0 μM) in the presence of different metal ions (500.0 μM). Inset: Corresponding fluorescence images. (B) The enhancement ratios I/I<sub>0</sub> versus metal ions. (C) SEM image of TPE-4CO<sub>2</sub>Na (20.0 μM) in the presence of Al<sup>3+</sup> (500.0 μM). (D) SEM image of TPE-4CO<sub>2</sub>Na (20.0 μM) in the presence of Pb<sup>2+</sup> (500.0 μM).

them were fully purified and characterized using  $^1\text{H}$  NMR,  $^{13}\text{C}$  NMR and MS (Figs. S1–S12).

The probe TPE-4CO<sub>2</sub>Na can dissolve very well in water, but hardly dissolve in common organic solvents such as THF. An aqueous solution of TPE-4CO<sub>2</sub>Na only has a very weak blue fluorescence, which is hardly observed by naked eye. Its fluorescence spectrum in Fig. 1 shows that its emission maximum is 400 nm when excited by the optimum excitation wavelength of 264 nm. Its lifetime was determined to be 0.7 ns from the time-resolved PL decay curve in Fig. S13. In contrast to its dissolved state, the solid powder of TPE-4CO<sub>2</sub>Na emits intense green light under the UV light. An apparent red-shift in emission maximum for TPE-4CO<sub>2</sub>Na powder was observed relative to that in dissolved state. The lifetime at 468 nm was lengthened to 2.1 ns determined from the time-resolved PL decay curve in Fig. S14. The quantum yield of TPE-4CO<sub>2</sub>Na powder was determined to 0.25 using an absolute method. The much higher emission efficiency of the solid state than the dissolved state provides an indication that TPE-4CO<sub>2</sub>Na possesses a significant AIE behavior. This AIE property was further verified by aggregation processes caused by a poor solvent and pH change in aqueous solution. A gradual enhancement trend in PL intensity of TPE-4CO<sub>2</sub>Na solutions was observed in Fig. 2A as the amount of THF in the mixed solutions was increased from 0% to 98%. As the continuous addition of THF into an aqueous TPE-4CO<sub>2</sub>Na solution, the solutions became more and more turbid accompanying more and more intense fluorescence, clearly suggesting unique AIE property of TPE-4CO<sub>2</sub>Na. The influence of TPE-4CO<sub>2</sub>Na by pH was shown in Fig. 2B. The TPE-4CO<sub>2</sub>Na solution remained

weakly emissive at pH > 5.0, but the fluorescence of the TPE-4CO<sub>2</sub>Na solution was progressively intensified as the decrease of pH from pH 5.0 to pH 1.0. The pH-triggered fluorescence enhancement was due to the aggregation of protonated form of TPE-4CO<sub>2</sub>Na. In comparison with preceding AIE probes [24–31], TPE-4CO<sub>2</sub>Na remained very weakly emissive in neutral water without the assistance of organic solvents. The PL spectra and lifetime of the acid form of the probe were also examined for comparison. Fig. S15 showed that the emission maximum of TPE-4CO<sub>2</sub>H was relatively blue-shifted to 436 nm, and its lifetime (2.2 ns) was comparable to that of the probe. These observations demonstrated that TPE-4CO<sub>2</sub>Na exhibited prominent AIE behavior and had excellent water solubility, avoiding false signals from self-precipitation in aqueous solution.

### 3.2. Discriminative detection of Al<sup>3+</sup> and Pb<sup>2+</sup> based on ion-triggered AIE

The PL responses of TPE-4CO<sub>2</sub>Na to 16 commonly used metal ions including K<sup>+</sup>, Mg<sup>2+</sup>, Ca<sup>2+</sup>, Ba<sup>2+</sup>, Al<sup>3+</sup>, Pb<sup>2+</sup>, Cd<sup>2+</sup>, Co<sup>2+</sup>, Fe<sup>2+</sup>, Ag<sup>+</sup>, Zn<sup>2+</sup>, Hg<sup>2+</sup>, Cu<sup>2+</sup>, Mn<sup>2+</sup>, Cr<sup>3+</sup> and Fe<sup>3+</sup> were first assessed as shown in Fig. 3A. Only the addition of Al<sup>3+</sup> (650.0 μM) or Pb<sup>2+</sup> (500.0 μM) caused a significant PL enhancement of TPE-4CO<sub>2</sub>Na, and a bright green emission can be readily observed by naked eye after the introduction of Al<sup>3+</sup> or Pb<sup>2+</sup>. The equivalent amount of Al<sup>3+</sup> resulted in much brighter fluorescence than Pb<sup>2+</sup>, which was clearly reflected by their respective PL enhancing ratios (186 for Al<sup>3+</sup>, 111 for Pb<sup>2+</sup>) in Fig. 3B. The quantum yield of TPE-4CO<sub>2</sub>Na after binding with Al<sup>3+</sup> was determined

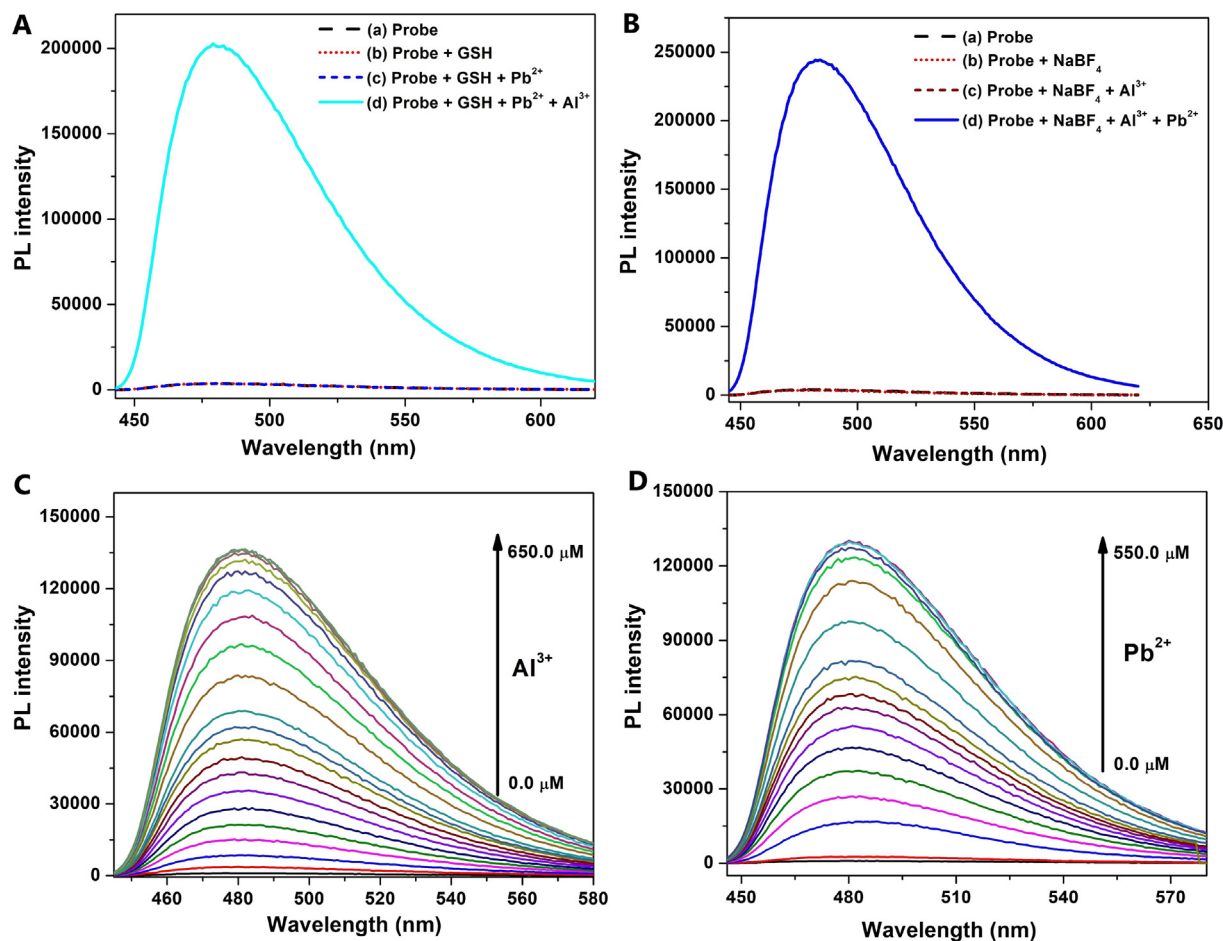


**Fig. 4.** (A) PL spectra of the probe TPE-4CO<sub>2</sub>Na in the presence of different components: (a) the probe (20.0 μM); (b) the probe (20.0 μM) and GSH (100.0 μM); (c) the probe (20.0 μM), GSH (100.0 μM) and Pb<sup>2+</sup> (100.0 μM); (d) the probe (20.0 μM), GSH (100.0 μM), Pb<sup>2+</sup> (100.0 μM) and Al<sup>3+</sup> (100.0 μM). (B) PL spectra of the probe TPE-4CO<sub>2</sub>Na in the presence of different components: (a) the probe (20.0 μM); (b) the probe (20.0 μM) and NaBF<sub>4</sub> (100.0 μM); (c) the probe (20.0 μM), NaBF<sub>4</sub> (100.0 μM) and Al<sup>3+</sup> (100.0 μM); (d) the probe (20.0 μM), NaBF<sub>4</sub> (100.0 μM), Al<sup>3+</sup> (100.0 μM) and Pb<sup>2+</sup> (100.0 μM). (C) PL spectra versus the concentration of Al<sup>3+</sup> from 0.0 to 650.0 μM. (D) PL spectra versus the concentration of Pb<sup>2+</sup> from 0.0 to 500.0 μM.

to be 25.7%, which was 180 times higher than the quantum yield of TPE-4CO<sub>2</sub>Na in solution (0.14%). We assumed that these PL enhancements caused by Al<sup>3+</sup> and Pb<sup>2+</sup> were due to the generation of aggregates between metal ions and TPE-4CO<sub>2</sub>Na via coordination. This assumption was verified by SEM images in Fig. 3C and D, where a great deal of large aggregates in millimeter magnitude was generated. These results provided solid evidence that the presence of Al<sup>3+</sup> or Pb<sup>2+</sup> triggered the generation of large aggregates of TPE-4CO<sub>2</sub>Na with intense green fluorescence, and offered the opportunity to establish quantitative detection method of Al<sup>3+</sup> and Pb<sup>2+</sup>.

Because both Al<sup>3+</sup> and Pb<sup>2+</sup> are capable of lighting up the probe TPE-4CO<sub>2</sub>Na, mutual interference can occur during the detection. As a result, we attempted to use masking reagents to minimize mutual interference between them. It was found that glutathione can tightly bind to Pb<sup>2+</sup> but exerts no significant interaction with Al<sup>3+</sup>, and thus glutathione was chosen as an effective masking agent to avoid the interference from Pb<sup>2+</sup> during the detection of Al<sup>3+</sup>. Fig. 4A shows the addition of single glutathione or the equivalent of glutathione and Pb<sup>2+</sup> causes no PL response, but continuous addition of the same amount of Al<sup>3+</sup> results in a sharp increase of PL intensity. This indicates that the introduction of glutathione effectively masks the added Pb<sup>2+</sup> without any impact on Al<sup>3+</sup>-triggered PL enhancement. In the same way, we found that NaBF<sub>4</sub> can eliminate the interference from Al<sup>3+</sup> during the detection of Pb<sup>2+</sup>. Fig. 4B illustrates the outstanding masking effect of NaBF<sub>4</sub> to Al<sup>3+</sup> and a good PL response to Pb<sup>2+</sup> in the presence of NaBF<sub>4</sub> and Al<sup>3+</sup>. With the assistance of masking reagents GSH and NaBF<sub>4</sub>, discriminative detection of Al<sup>3+</sup> and Pb<sup>2+</sup> can be readily achieved using TPE-4CO<sub>2</sub>Na. Fig. 4C shows a gradual PL enhancement of TPE-4CO<sub>2</sub>Na as the continuous addition of Al<sup>3+</sup> in the range of 0.0–650.0 μM, and a good linear relationship between PL intensity and Al<sup>3+</sup> concentration in the range of 20.0–400.0 μM is obtained (Fig. S16). The detection limit according to this calibration curve was estimated to 0.7 μM. According to Table S1, the detection limit is inferior to those of several preceding AIEgen-based methods

(6.2–21.6 nM) [29], but is better than those of most approaches based on AIEgens (1.5–5.3 μM) [24,25,27,30] and ACQ fluorophores (1.0–21.7 μM) [35–38]. The appreciable decline in response sensitivity of our method is due to the large solubility of TPE-4CO<sub>2</sub>Na in water, and this sacrifice in sensitivity is acceptable under the premise of avoiding the false signal from self-precipitation due to low water-solubility. A similar PL increase trend with the concentration of Pb<sup>2+</sup> from 0.0 to 500.0 μM was shown in Fig. 4D, and calibration curve between PL intensity and Pb<sup>2+</sup> concentration ranging from 2.0 to 300.0 μM was acquired (Fig. S17). The detection limit for Pb<sup>2+</sup> was calculated to be 0.6 μM, and this value is comparable to those of fluorescent methods in the literature [7,39].

### 3.3. Live cell imaging of aluminum ions in *Arabidopsis thaliana*

Discriminative detection of aluminum ions over lead ions in the presence of glutathione based on TPE-4CO<sub>2</sub>Na enables us to specifically image Al<sup>3+</sup> in live cells because of the occurrence of a high amount of glutathione inside living cells [40,41]. *Arabidopsis thaliana* as a typical model plant was selected to examine the imaging performance of TPE-4CO<sub>2</sub>Na in live cells [42,43]. Five-day old seedlings of *Arabidopsis thaliana* was used because their transparent roots are suited for the penetration of visible excitation and emission light. We first assessed the cell permeability and imaging ability of water-soluble TPE-4CO<sub>2</sub>Na. As shown in Fig. S18, the root cells of *Arabidopsis thaliana* seedling treated with TPE-4CO<sub>2</sub>Na exhibits a very weak autofluorescence as same as the mock control has, but an apparent pseudo green color from the root tips can be observed after continuous treatment of the seedlings with TPE-4CO<sub>2</sub>Na and Al<sup>3+</sup>. This faint fluorescence signal implies that water-soluble TPE-4CO<sub>2</sub>Na is cell-permeable but the accumulation amount in cells in a short time (10 min) is very small. To facilitate the cell permeability of the probe, its acidic form TPE-4CO<sub>2</sub>H was used in a mixed solvent. Fig. 5 shows laser scanning confocal microscopy images of

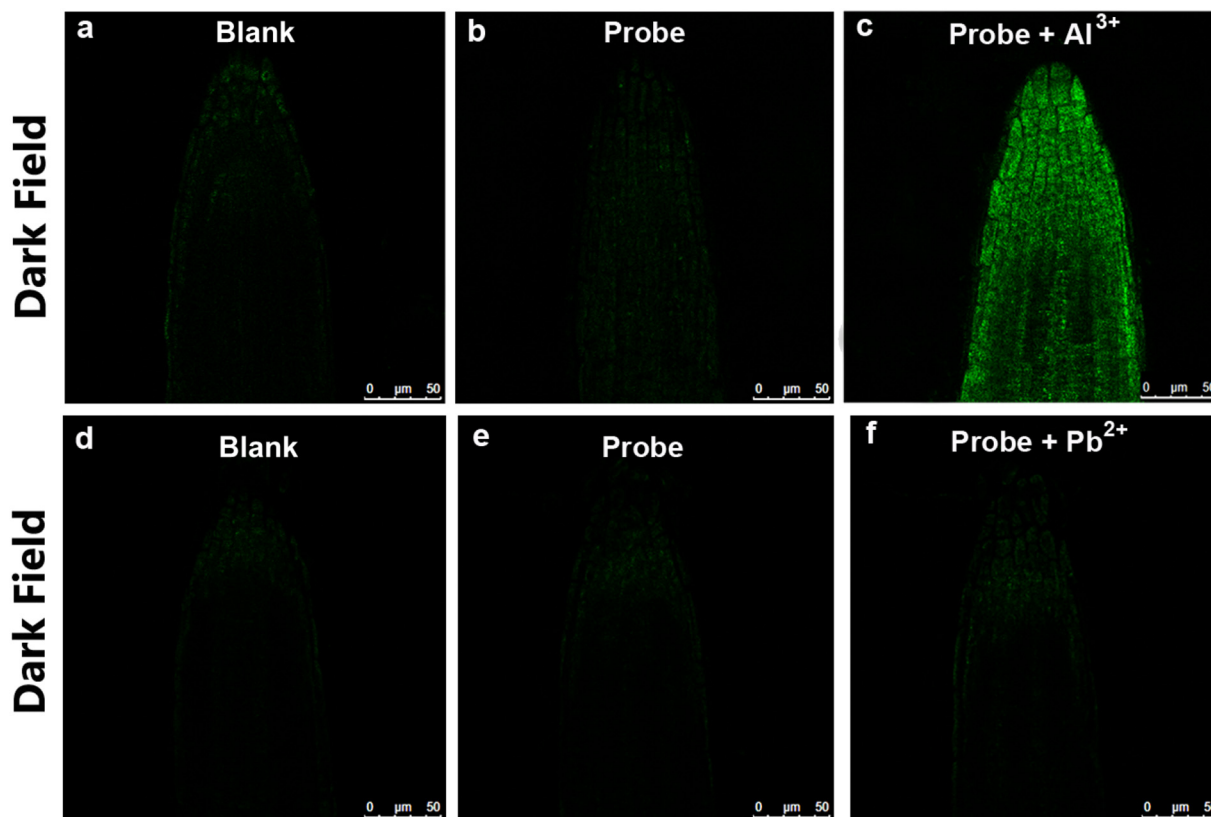


Fig. 5. Laser scanning confocal microscopy images in seedling roots of *Arabidopsis thaliana* under different conditions: (a, d) mock control; (b, e) incubated with TPE-4CO<sub>2</sub>H (0.5 mM) for 30 s; (c) incubated with TPE-4CO<sub>2</sub>H (0.5 mM) and Al<sup>3+</sup> (0.5 mM) for 30 s; (f) incubated with TPE-4CO<sub>2</sub>H (0.5 mM) and Pb<sup>2+</sup> (0.5 mM) for 30s.

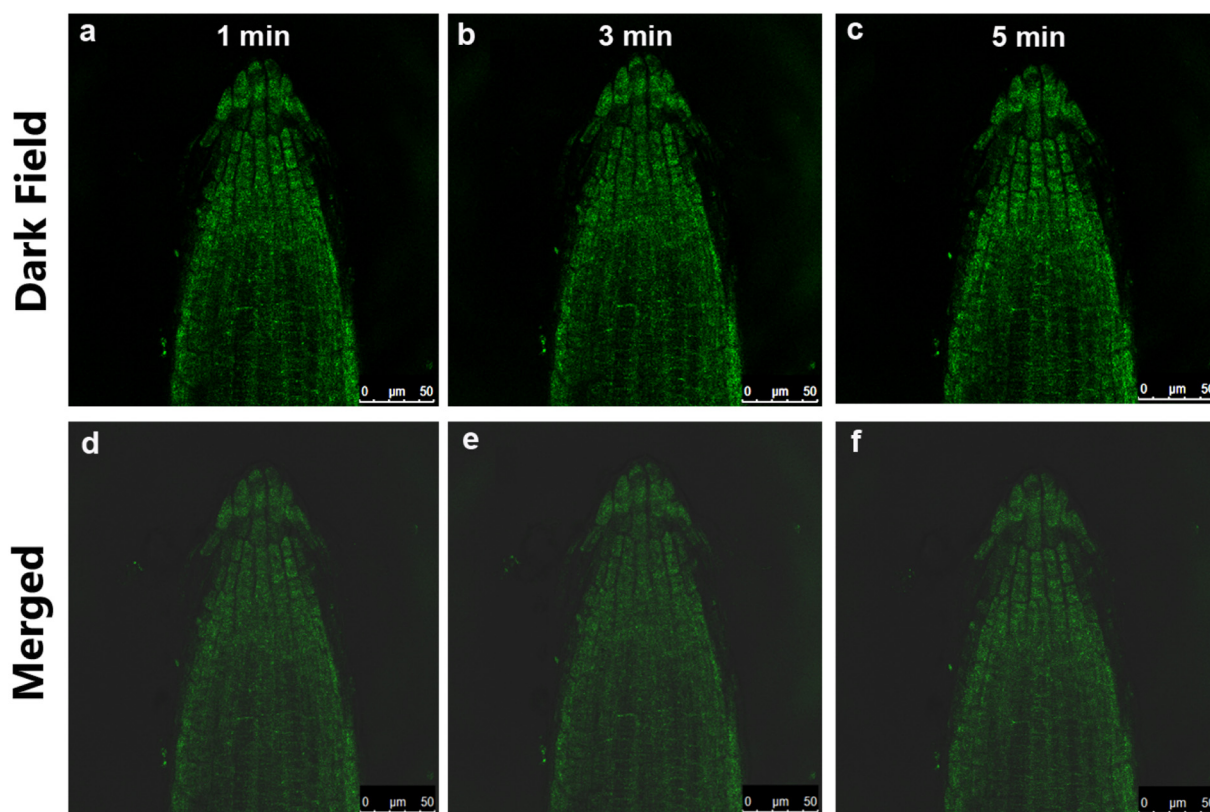


Fig. 6. Laser scanning confocal microscopy images of seedling roots of *Arabidopsis thaliana* radiated with different time lengths. (a, d) 1 min, (b, e) 3 min, (c, f) 5 min.

different groups of seedling roots. Almost no fluorescence signal was recorded for mock control under the given set of conditions, and only very weak fluorescence was observed for root cells of *Arabidopsis* seedlings treated with TPE-4CO<sub>2</sub>H, indicating that TPE-4CO<sub>2</sub>H will not aggregate under the physiological conditions inside living cells. Continuous incubation of the seedlings with a given concentration of Al<sup>3+</sup> for a short time (10 min) resulted in a bright green fluorescence, and almost all the cells were clearly labeled with intense green color. However, the introduction of comparable amount of Pb<sup>2+</sup> to Al<sup>3+</sup> did not lead to the generation of intense emission signals. These results show that TPE-4CO<sub>2</sub>H is capable of discriminatively imaging Al<sup>3+</sup> over Pb<sup>2+</sup> due to the existence of abundant glutathione inside living cells. The photostability of TPE-4CO<sub>2</sub>H was further evaluated after bound with aluminum ions. Fig. 6 shows fluorescence intensity changes as the elongation of irradiation time from 1 to 5 min. It is found that there is no apparent decline in fluorescence intensity and no appreciable photobleaching occurs in a given time course by comparing the laser scanning confocal microscopy images, indicating that the probe has good photostability and can be suited for long-term imaging.

#### 4. Conclusion

In summary, a water-soluble molecular probe that is capable of discriminative detection of aluminum ion and lead ion based on ion-triggered aggregation-induced emission is reported. The molecular probe was composed of a tetraphenylethylene unit and four carboxylic acid groups, and the introduction of four carboxylic acid groups facilitates the water-solubility of designed probe to avoid the self-precipitation in aqueous solution. The probe shows specific response to aluminum ion and lead ion in a fluorescence turn-on manner due to high binding affinities of four carboxylic acid groups to aluminum ion and lead ion. With the assistance of different masking reagents, this probe can be used to discriminate aluminum ion and lead ion in qualitative and quantitative way. Live-cell imaging results demonstrate

that the acidic form of the probe is cell-permeable and is capable of selectively imaging aluminum ions in living cells. The excellent photostability of fluorescent aggregates consisting of the probe and aluminum ion illustrates that the designed probe is suited for long-term imaging of ions without appreciable photobleaching.

#### Acknowledgements

We gratefully acknowledge the financial support from the National Natural Science Foundation of China (Grant Nos. 21675143, 21775139 and 21775138), and Natural Science Foundation of Zhejiang Province (Grant Nos. LR18B050001 and LY17B050003).

#### Appendix A. Supplementary data

Supplementary data to this article can be found online at <https://doi.org/10.1016/j.saa.2019.117335>.

#### References

- [1] G. Furrer, B.L. Phillips, K.-U. Ulrich, R. Pothig, W.H. Casey, The origin of aluminum flocs in polluted streams, *Science* 297 (2002) 2245–2247.
- [2] R.J. Mailloux, J. Lemire, V.D. Appanna, Hepatic response to aluminum toxicity: dyslipidemia and liver diseases, *Exp. Cell Res.* 317 (2011) 2231–2238.
- [3] H. Sade, B. Meriga, V. Surapu, J. Gadi, M.S.L. Sunita, P. Suravajhala, et al., Toxicity and tolerance of aluminum in plants: tailoring plants to suit to acid soils, *Biometal* 29 (2016) 187–210.
- [4] M. Ahamed, M.K.J. Siddiqui, Environmental lead toxicity and nutritional factors, *Clin. Nutr.* 26 (2007) 400–408.
- [5] A. Kumar, M.N.V. Prasad, Plant-lead interactions: transport, toxicity, tolerance, and detoxification mechanisms, *Ecotox Environ Safe* 166 (2018) 401–418.
- [6] A. Gupta, N. Kumar, A review of mechanisms for fluorescent “turn-on” probes to detect Al<sup>3+</sup> ions, *RSC Adv.* 6 (2016) 106413–106434.
- [7] H.N. Kim, W.X. Ren, J.S. Kim, J. Yoon, Fluorescent and colorimetric sensors for detection of lead, cadmium, and mercury ions, *Chem. Soc. Rev.* 41 (2012) 3210–3244.
- [8] R.T.K. Kwok, C.W.T. Leung, J.W.Y. Lam, B.Z. Tang, Biosensing by luminogens with aggregation-induced emission characteristics, *Chem. Soc. Rev.* 44 (2015) 4228–4238.

- [9] J. Mei, N.L.C. Leung, R.T.K. Kwok, J.W.Y. Lam, B.Z. Tang, Aggregation-induced emission: together we shine, united we soar, *Chem. Rev.* 115 (2015) 11718–11940.
- [10] Y. Hong, J.W.Y. Lam, B.Z. Tang, Aggregation-induced emission, *Chem. Soc. Rev.* 40 (2011) 5361–5388.
- [11] M. Gao, B.Z. Tang, Fluorescent sensors based on aggregation-induced emission: recent advances and perspectives, *ACS Sens* 2 (2017) 1382–1399.
- [12] D.D. La, S.V. Bhosale, L.A. Jones, S.V. Bhosale, Tetraphenylethylene-based AIE-active probes for sensing applications, *ACS Appl. Mater. Interfaces* 10 (2018) 12189–12216.
- [13] Y.F. Wang, T. Zhang, X.J. Liang, Aggregation-induced emission: lighting up cells, revealing life, *Small* 12 (2016) 6451–6477.
- [14] L. Liu, G. Zhang, J. Xiang, D. Zhang, D. Zhu, Fluorescence “turn on” chemosensors for  $\text{Ag}^+$  and  $\text{Hg}^{2+}$  based on tetraphenylethylene motif featuring adenine and thymine moieties, *Org. Lett.* 10 (2008) 4581–4584.
- [15] S. Umar, A.K. Jha, D. Purohit, A. Goel, A tetraphenylethylene-naphthylridine-based AIEgen TPEN with dual mechanochromic and chemosensing properties, *J Org Chem* 82 (2017) 4766–4773.
- [16] Y. Chen, W. Zhang, Y. Cai, R.T.K. Kwok, Y. Hu, J.W.Y. Lam, et al., AIEgens for dark through-bond energy transfer: design, synthesis, theoretical study and application in ratiometric  $\text{Hg}^{2+}$  sensing, *Chem. Sci.* 8 (2017) 2047–2055.
- [17] Z. Ruan, C. Li, J.R. Li, J. Qin, Z. Li, A relay strategy for the mercury(II) chemodosimeter with ultrasensitivity as test strips, *Sci. Rep.* 51 (2015) 15987.
- [18] M.T. Gabr, F.C. Pigge, A selective fluorescent sensor for  $\text{Zn}^{2+}$  based on aggregation-induced emission (AIE) activity and metal chelating ability of bis(2-pyridyl)-diphenylethylene, *Dalton Trans.* 45 (2016) 14039–14043.
- [19] H. Mehdi, W. Gong, H. Guo, M. Watkinson, H. Ma, A. Wajahat, et al., Aggregation-induced emission (AIE) fluorophore exhibits a highly ratiometric fluorescent response to  $\text{Zn}^{2+}$  in vitro and in human liver cancer cells, *Chem. Eur. J.* 23 (2017) 13067–13075.
- [20] M. Shyamal, P. Mazumdar, S. Maity, S. Samanta, G.P. Sahoo, A. Misra, Highly selective turn-on fluorogenic chemosensor for robust quantification of  $\text{Zn(II)}$  based on aggregation induced emission enhancement feature, *ACS Sens* 1 (2016) 739–747.
- [21] F. Sun, G. Zhang, D. Zhang, L. Xue, H. Jiang, Aqueous fluorescence turn-on sensor for  $\text{Zn}^{2+}$  with a tetraphenylethylene compound, *Org. Lett.* 13 (2011) 6378–6381.
- [22] M. Gao, Y. Li, X. Chen, S. Li, L. Ren, B.Z. Tang, Aggregation-induced emission probe for light-up and in situ detection of calcium ions at high concentration, *ACS Appl. Mater. Interfaces* 10 (2018) 14410–14417.
- [23] J. Zhang, Z. Yan, S. Wang, M. She, Z. Zhang, W. Cai, et al., Water soluble chemosensor for  $\text{Ca}^{2+}$  based on aggregation-induced emission characteristics and its fluorescence imaging in living cells, *Dyes Pigments* 150 (2018) 112–120.
- [24] T. Han, X. Feng, B. Tong, J. Shi, L. Chen, J. Zhi, et al., A novel “turn-on” fluorescent chemosensor for the selective detection of  $\text{Al}^{3+}$  based on aggregation-induced emission, *Chem. Commun.* 48 (2012) 416–418.
- [25] P. Liu, W. Li, S. Guo, D. Xu, M. Wang, J. Shi, et al., Application of a novel “turn-on” fluorescent material to the detection of aluminum ion in blood serum, *ACS Appl. Mater. Interfaces* 10 (2018) 23667–23673.
- [26] N. Na, F. Wang, J. Huang, C. Niu, C. Yang, Z. Shang, et al., J, an aggregation-induced emission-based fluorescent chemosensor of aluminum ions, *RSC Adv.* 4 (2014) 35459–35462.
- [27] S. Samanta, S. Goswami, M.N. Hoque, A. Ramesh, G. Das, An aggregation-induced emission (AIE) active probe renders  $\text{Al(III)}$  sensing and tracking of subsequent interaction with DNA, *Chem. Commun.* 50 (2014) 11833–11836.
- [28] S. Samanta, U. Manna, T. Ray, G. Das, An aggregation-induced emission (AIE) active probe for multiple targets: a fluorescent sensor for  $\text{Zn}^{2+}$  and  $\text{Al}^{3+}$  and a colorimetric sensor for  $\text{Cu}^{2+}$  and  $\text{F}^-$ , *Dalton Trans.* 44 (2015) 18902–18910.
- [29] K. Santhiya, S.K. Sen, R. Natarajan, R. Shankar, B. Murgesapandian, D-A-D structured bis-acylhydrazone exhibiting aggregation-induced emission, mechanochromic luminescence, and  $\text{Al(III)}$  detection, *J Org Chem* 83 (2018) 10770–10775.
- [30] X. Shi, H. Wang, T. Han, X. Feng, B. Tong, J. Shi, et al., A highly sensitive, single selective, real-time and “turn-on” fluorescent sensor for  $\text{Al}^{3+}$  detection in aqueous solution, *J. Mater. Chem.* 22 (2012) 19296–19302.
- [31] T. Wei, J. Zhang, G. Mao, X. Zhang, Z. Ran, W. Tan, et al., An efficient fluorescence turn-on probe for  $\text{Al}^{3+}$  based on aggregation-induced emission, *Anal. Methods*, 5 (2013) 3909–3914.
- [32] D.G. Khandare, H. Joshi, M. Banerjee, M.S. Majik, A. Chatterjee, An aggregation-induced emission based “turn-on” fluorescent chemodosimeter for the selective detection of  $\text{Pb}^{2+}$  ions, *RSC Adv.* 4 (2014) 47076–47080.
- [33] X. Li, B. Xu, H. Lu, Z. Wang, J. Zhang, Y. Zhang, et al., Label-free fluorescence turn-on detection of  $\text{Pb}^{2+}$  based on AIE-active quaternary ammonium salt of 9,10-distyrylanthracene, *Anal. Methods* 5 (2013) 438–441.
- [34] S.K. Saha, K.R. Ghosh, J.P. Gao, Z.Y. Wang, Highly sensitive dual-mode fluorescence detection of lead ion in water using aggregation-induced emissive polymers, *Macromol. Rapid Commun.* 35 (2014) 1592–1597.
- [35] S. Erdemir, S. Malkondu, A simple triazole-based “turn on” fluorescent sensors for  $\text{Al}^{3+}$  in  $\text{MeCN-H}_2\text{O}$  and  $\text{F}^-$  ion in  $\text{MeCN}$ , *J. Lumin.* 158 (2015) 401–406.
- [36] J.C. Qin, Z.Y. Yang, P. Yang, Recognition of  $\text{Al}^{3+}$  based on a naphthalene-based “off-on” chemosensor in near 100% aqueous media, *Inorg Chem Acta* 432 (2015) 136–141.
- [37] G.T. Selvan, M. Kumaresan, R. Sivaraj, I.V.M.V. Enoch, P.M. Selvakumar, Isomeric 4-aminoantipyrene derivatives as fluorescent chemosensors of  $\text{Al}^{3+}$  ions and their molecular logic behaviour, *Sensor Actuat B-Chem* 229 (2016) 181–189.
- [38] J. Zhao, Y. Zhao, S. Xu, N. Luo, R. Tang, A selective fluorescent probe for relay recognition of  $\text{Al}^{3+}$  and  $\text{Cu}^{2+}$  through fluorescence “off-on-off” functionality, *Inorg. Chim. Acta* 438 (2015) 105–111.
- [39] G. Chen, Z. Guo, G. Zeng, L. Tang, Fluorescent and colorimetric sensors for environmental mercury detection, *Analyst* 140 (2015) 5400–5443.
- [40] X. Jiang, J. Chen, A. Bajic, C. Zhang, X. Song, S.L. Carroll, et al., Quantitative real-time imaging of glutathione, *Nat. Commun.* 8 (2017) 16087.
- [41] C.X. Yin, K.M. Xiong, F.J. Huo, J.C. Salzman, R.M. Strongin, Fluorescent probes with multiple binding sites for the discrimination of Cys, Hcy, and GSH, *Angew. Chem. Int. Ed.* 56 (2017) 13188–13198.
- [42] M. Koornneef, D. Meinke, The development of Arabidopsis as a model plant, *Plant J.* 61 (2010) 909–921.
- [43] D.W. Meinke, J.M. Cherry, C. Dean, S.D. Rounsley, M. Koornneef, Arabidopsis thaliana: a model plant for genome analysis, *Science* 282 (1998) 679–682.